

Radar Human Motion Classification Using Multi-Antenna System

Patrick A Schooley and Syed A. Hamza

School of Engineering, Widener University, Chester, PA 19013, USA

ABSTRACT

This paper considers human activity classification for an indoor radar system. Human motions generate non-stationary radar returns which represent Doppler and micro-Doppler signals. The time-frequency (TF) analysis of micro-Doppler signals can discern subtle variations on the motion by precisely revealing velocity components of various moving body parts. We consider radar for activity monitoring using TF-based machine learning approach exploiting both temporal and spatial degrees of freedom. The proposed approach captures different human motion representations more vividly in joint-variable data domains achieved through beamforming at the receiver. The radar data is collected using real time measurements at 77 GHz using four receive antennas, and subsequently micro-Doppler signatures are analyzed through machine learning algorithm for classifications of human walking motions. We present the performance of the proposed multi antenna approach in separating and classifying two closely walking persons moving in opposite directions.

1. INTRODUCTION

Human motion recognition (HMR) finds important applications in a large variety of scenarios ranging from gesture recognition for smart homes, detecting events of interest for automatic surveillance, behavioral analysis, Gait abnormality recognitions, health monitoring in care facilities and rehabilitation services to enable independent living for elderly.¹⁻⁶

Contactless sensing of human motions has gained traction because of the obvious benefits of being non obtrusive. It does not require any user intervention and as such the users are not required to wear specific devices to be tracked via smart phone applications.⁷⁻⁹ Radar systems are at the forefront of remote sensing technologies as they provide robust non contact monitoring that is not affected by lighting conditions. Additionally, active RF (radio frequency) sensing provides 4D imaging capabilities by explicitly measuring the scatterer velocity in addition to range and 2D angular localization. This is unlike other remote sensing sensors of human motions such as visual-based systems that require additional pre-processing and filtering operations to accurately discern small movements.^{10,11} Also radar images are privacy preserving as high resolution imaging radar renders silhouette type portrait revealing little identifiable information as opposed to camera-based systems.

We investigate a human activity monitoring system to concurrently monitor movements of multiple persons. This could facilitate to separately record the activities of multiple persons in detail. For example, in health care facility, the task of care givers can be eased by attending to the needs of several care receivers at the same time. Radar is a proven technology for target detection, localization and tracking. Imaging radars are getting attention recently because of their added capability of classifying different targets. Radar returns classification could be performed after localizing the target in range, azimuth and/or Doppler.

In this paper, we consider the radar human motion classification by attempting to localize the motions to a given azimuth directions. The proposed beamforming approach can reduce the system cost and alleviate the need of using multiple radars as proposed in.^{10,12-14} Azimuth filtering is achieved by applying beamforming to the receiver array. Specifically, we consider the task of classifying two persons walking closely in opposite directions at different azimuth angles. We aim to correctly pair the direction of motion to the corresponding azimuth angle. This is achieved by jointly processing the two spectrograms obtained in the directions of both motions. In this case, the received data is filtered using beamforming with two separate sets of beamformer

E-mails: {paschooley, shamza}@widener.edu

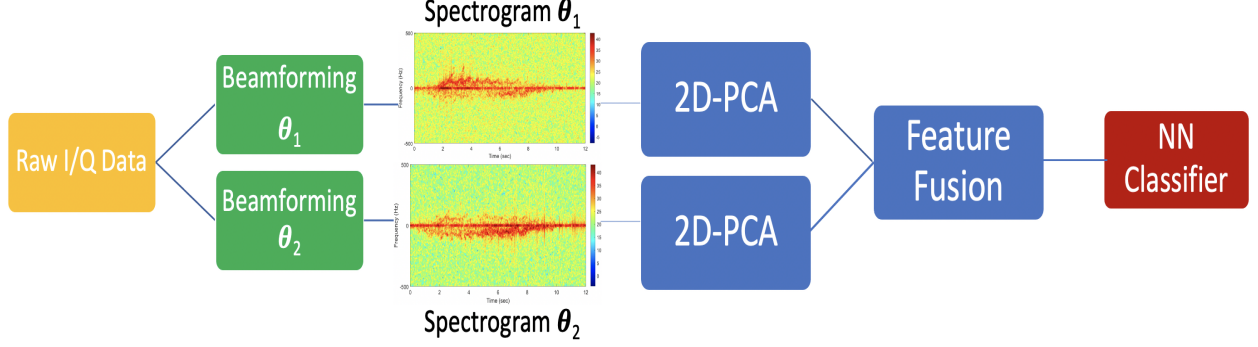


Figure 1. Processing sequence

weights. Subsequently, classification is performed by jointly processing the time frequency signature of both azimuth directions. The proposed scheme works adequately when the two motions are not completely separable in azimuth. This could either be due to the close proximity of the two motions in the azimuth or high sidelobes of the beamformer.

The rest of the paper is organized as follows: In the next section, we describe the data set and time frequency representation domain. The 2D PCA and beamformer image fusion for multi-person monitoring is discussed in Section 3. Experimental results are shown in Section 4, while the conclusion is given in Section 5.

2. RADAR RETURN SIGNAL ANALYSIS

The complex valued raw data matrix $\mathbf{s}(n, m) \in \mathbb{C}^{N \times M}$ of the frequency-modulated continuous wave (FMCW) radar is obtained through spatially processing the radar returns by an M element uniformly spaced antenna array. The data is collected over N temporal sampling instances. The receiver array vector $\mathbf{s}(m) \in \mathbb{C}^M$ at time instant n corresponds to the n_{th} row of $\mathbf{s}(n, m)$ and is given by,

$$\mathbf{s}(m) = \sum_{l=1}^L \alpha_l \mathbf{a}(\theta_l) + \mathbf{v}(m), \quad (1)$$

where, $\mathbf{a}(\theta_l) \in \mathbb{C}^M$ is the steering vector corresponding to the azimuth direction θ_l of the scatterer, and is defined as follows,

$$\mathbf{a}(\theta_l) = [1 \ e^{j(2\pi/\lambda)d\cos(\theta_l)} \ \dots \ e^{j(2\pi/\lambda)d(M-1)\cos(\theta_l)}]^T. \quad (2)$$

Here, d is the inter-element spacing and $\alpha_l \in \mathbb{C}$ is the complex amplitude of the radar return. The additive Gaussian noise $\mathbf{v}(m) \in \mathbb{C}^M$ has variance σ_v^2 . The elements of the received data vector $\mathbf{s}(m)$ are combined linearly by the M -sensor beamformer that strives to spatially filter the reflections from all other directions except the signal in the direction of beamformer look angle θ_k . The spatially filtered signal vector $\mathbf{x}(\theta_k) \in \mathbb{C}^N$ after beamforming is given by,

$$\mathbf{x}(\theta_k) = \mathbf{s}(n, m) \mathbf{w}^H(\theta_k), \quad (3)$$

where $\mathbf{w}(\theta_k) = \mathbf{a}^H(\theta_k)$ are the complex beamformer weights pointing towards θ_k .

The spatially filtered signal vector $\mathbf{x}(\theta_k)$ is reshaped into a two-dimensional matrix, $\mathbf{x}_{\theta_k}(p, q)$. This is achieved by segmenting the N dimensional vector $\mathbf{x}(\theta_k)$, such that, the P samples collected within a pulse repetition interval (PRI) are stacked into a P dimensional column. There are Q such columns within $\mathbf{x}_{\theta_k}(p, q)$ where $Q = N/P$ is the number of PRIs processed within the observation time N . The range-map, $\mathbf{r}_{\theta_k}(p, q)$ is obtained by applying the column-wise Discrete Fourier Transform (DFT) operation which is given by,

$$\mathbf{r}_{\theta_k}(l, q) = \sum_{p=0}^{P-1} \mathbf{x}_{\theta_k}(p, q) e^{-j(2\pi lp/N)} \quad (4)$$

We observe the data in the TF domain after localizing the motion in azimuth and range bins of interest. The spectrogram is used as the TF signal representation, showing the variation of the signal power as a function of time n and frequency k . The spectrogram of a periodic version of a discrete signal $\mathbf{v}_{\theta_k}(n)$, is given by,^{15–17}

$$\mathbf{d}_{\theta_k}(n, k) = \left| \sum_{m=0}^{H-1} \mathbf{h}(m) \mathbf{v}_{\theta_k}(n-m) e^{-j(2\pi km/H)} \right|^2, \quad (5)$$

where $\mathbf{v}_{\theta_k} = \sum_{l=r_l}^{r_u} \mathbf{r}_{\theta_k}(l, q)$ is obtained by collapsing the range dimension beginning from lower range bin r_l to highest range bin r_h . Tapering window \mathbf{h} of length H is applied to reduce the sidelobes. The spectrograms reveal the the different velocities, accelerations and higher order moments which cannot be easily modeled or assumed to follow specific nonstationary structures.¹⁸ We observe the motion of two humans walking closely in opposite directions at different azimuth angles. We aim to correctly pair the direction of motion to the corresponding azimuth angle. This is achieved by jointly processing two spectrograms, $\mathbf{v}_{\theta_1}(n, k)$ and $\mathbf{v}_{\theta_2}(n, k)$ which are respectively localized at azimuth angles θ_1 and θ_2 . It is clear that the concurrent motions of multiple objects are hard to be distinguished in azimuth by only using a single antenna.

3. FEATURE EXTRACTION AND CLASSIFICATION

We adopt Two-Dimensional Principal Component Analysis (2-D PCA) for dimensionality reduction to draw the most pertinent features from spectrograms.^{19,20} The features obtained from individual spectrograms are jointly classified with the Nearest Neighbor (NN) classifier.²¹

The 2-D PCA is performed on the covariance matrix \mathbf{R}_{θ_k} which is computed as follows,

$$\mathbf{R}_{\theta_k} = \sum_{i=0}^{T-1} \mathbf{X}_{\theta_k}^{iH} \mathbf{X}_{\theta_k}^i, \quad (6)$$

where, $\mathbf{X}_{\theta_k}^i$ is the normalized spectrogram for the i_{th} example and T are the total training examples. The eigendecomposition of R_{θ_k} is performed and the individual train images are projected onto the subspace spanned by the K dominant eigenvectors of R_{θ_k} corresponding to the K largest eigenvalues. It is noted that two spectrogram images are generated per example, by using two different sets of beamformer weights. After separately performing the 2-D PCA, the projected spectrograms are vectorized and concatenated before training the NN classifier, as shown in Fig. 1.

The overall data collection, preprocessing and classification can be described by the following steps.

3.1 Data Collection and Preprocessing

- PRI is set to 1 ms, and each data example is observed over the time period of 12 s, resulting in $Q = 12000$ slow time samples.
- ADC sampling rate is 512 ksps, rendering 512 fast time samples per PRI, resultantly the length of data vector is $N = 6144000$.
- The received data $\mathbf{s}(n, m) \in C^{N \times M}$, is collected through $M = 4$ element receive array, with an inter-element spacing of $\lambda/2$ (λ is the wavelength corresponding to the operating frequency), therefore the dimensionality of received raw data matrix is 6144000×4 .
- Beamforming is performed on the raw data matrix, resulting in a spatially filtered $\mathbf{x}(\theta_k)$ vector of dimensions 6144000×1 . Two such vectors are generated in the directions of each motion θ_1 and θ_2 .
- Each vector $\mathbf{x}(\theta_k)$ is reshaped into a 512×12000 matrix. After applying columnwise DFT, and identifying the range bins of interest, the corresponding rows are summed together, resulting in $\mathbf{v}_{\theta_k} = \sum_{l=r_l}^{r_u} \mathbf{r}_{\theta_k}(l, q)$, which is of dimensions 12000×1 .
- Two spectrogram \mathbf{d}_{θ_1} and \mathbf{d}_{θ_2} , each of dimensions 384×128 is obtained, where the window length is 128.

3.2 Training

- Normalize both spectrograms of all training examples \mathbf{v}_{θ_k} by subtracting the average.
- Perform the eigendecomposition of the covariance matrices estimated according to (6) and select K dominant eigenvectors. Note that covariance matrices are separately evaluated for both angles.
- Project the training spectrograms onto the subspace spanned by selected eigenvectors, resulting in two projected spectrograms per example. Each has the dimensionality $128 \times K$.
- After vectorizing each spectrogram, both are concatenated into a $256K \times 1$ vector and trained through NN classifier.

3.3 Testing

- Normalize the testing image and project onto the subspace obtained in the training process.
- The testing image is then passed onto trained NN classifier for prediction.

Table 1. Confusion matrix, Number of principal eigenvectors, $K=1$

Classified/Actual Class	Class-1	Class-2
Class-1	97.6%	0%
Class-2	2.4%	100%

Table 2. Confusion matrix, Number of principal eigenvectors, $K=2$

Classified/Actual Class	Class-1	Class-2
Class-1	100%	0%
Class-2	0%	100%

4. EXPERIMENTAL RESULTS

In this section, we demonstrate the effectiveness of beamformer image fusion for monitoring multiple persons in the field of view. We consider two classes, Class-1 and Class-2, of motions. For Class-1 motions, one person moves radially towards the radar at an azimuth angle of θ_1 while at the same time another person moves radially away from the radar at an azimuth angle of θ_2 . For Class-2 motion, the two persons perform the same walking motion but in an opposite direction, i.e., this time the person at azimuth angle θ_1 moves radially away from the radar, whereas the other person concurrently moves radially towards the radar at an azimuth angle of θ_2 .

Figure 2 shows the time frequency signature of Class-1 motion. Note the TF domain depicts both strong positive and negative Doppler, where both frequencies are present at the same time. The time frequency signature of the Class-1 motion is processed after applying beamforming weights to the output of all receivers. The beamformer points to θ_1 direction. Figure 3 shows the time frequency signature of the beamformer pointing towards θ_1 . It is evident from the time frequency signature that the beamformer attempted to filter the positive frequencies. However, the positive Doppler is not completely eliminated due to the sidelobes of the beamformer. The beamformer pointing towards θ_2 emphasizes the positive Doppler while attempting to mitigate the strong negative Doppler as depicted in Fig. 4. On the other hand, Fig. 5 shows the TF spectrum of the Class-2 motion. It is clear that Figs. 2 and 5 are very similar and are of little use to classify the two motion classes. However, the spatially filtered TF spectrums for Class-2 are flipped for respective look directions when compared to Class-1 motion as shown in Figs. 6 and 7. Therefore, the two beamformed TF spectrums when processed jointly can

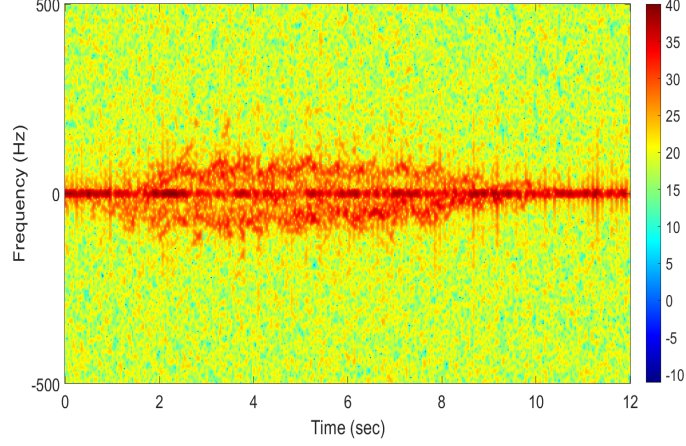


Figure 2. Time Frequency signature of Class-1 motions processed through single antenna (without beamforming)

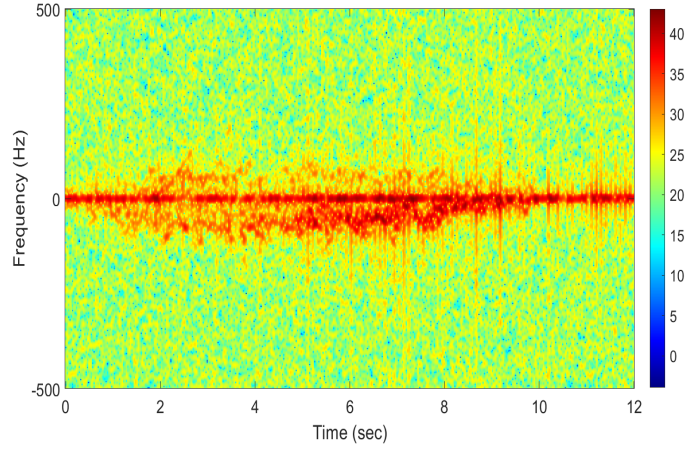


Figure 3. Time Frequency signature of Class-1 motions processed through beamformer pointing towards θ_1 .

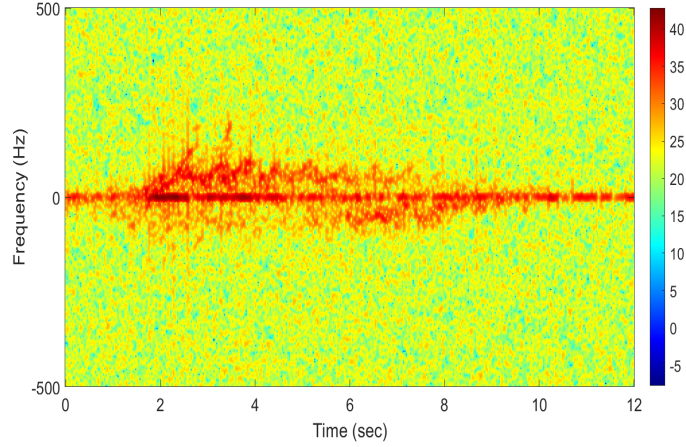


Figure 4. Time Frequency signature of Class-1 motions processed through beamformer pointing towards θ_2 .

potentially classify the two motion classes with reasonable accuracy, therefore mapping the direction of motion to the correct azimuth angle.

The radar system used in the experiments is AWR2243 from Texas Instruments having four receiver and three transmitters. The center frequency is 77 GHz, whereas the bandwidth is 5 GHz. The obtained data set is analyzed in MATLAB R2020B. The data set contains 120 samples, 60 samples for each motion class collected

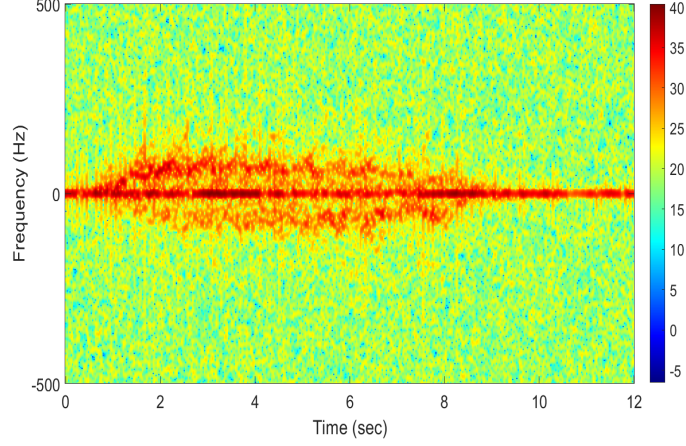


Figure 5. Time Frequency signature of Class-2 motions processed through single antenna (without beamforming)

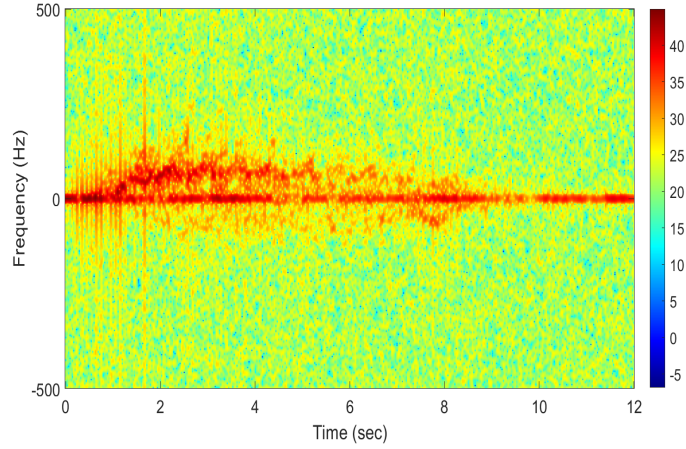


Figure 6. Time Frequency signature of Class-2 motions processed through beamformer pointing towards θ_1 .

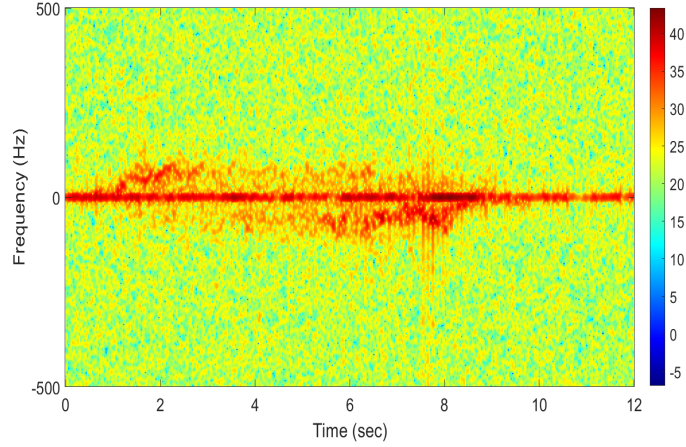


Figure 7. Time Frequency signature of Class-2 motions processed through beamformer pointing towards θ_2 .

through six subjects. For the 2D PCA-based classifications, the training set consists of 46 samples for each class (92 samples in total), and each sample are two 128×384 images. The rest of the data set is used for testing. The first image is generated by steering the beamformer to θ_1 . Likewise, the other image is generated by changing the steering angle to θ_2 . Thus, for each motion class two $128 \times 384 \times 46$ matrices are generated. After performing the dimensionality reduction through 2D PCA, both beamformed TF images are concatenated

together and passed on to NN classifier. The confusion matrix for fused spectrogram is shown in Tables 1, depicting the correspondence between the actual and the classified class. It shows that using only the dominant eigenvector renders a classification accuracy of around 97.6% and 100% for Class-1 and Class-2 respectively. More specifically, Table 1 depicts that the around 97.6% of actual Class-1 motions are classified as Class-1, while the rest 2.4% are declared as Class-2. The success rate can be improved by including an additional principal component. Table 2 shows that the proposed scheme has a 100% success rate when two principal eigenvectors are employed.

5. CONCLUSION

In this paper, we introduced an approach that observes the time frequency representation of radar returns from different azimuth angles. We provided an effective means to discern combinations of multiple motions occurring at different angular directions from the radar. The proposed approach successfully maps the actual motions to the corresponding angular locations and is found to be effective when the spectrograms are not completely separable in angle.

6. ACKNOWLEDGMENT

The authors would like to thank Andrew Lichtenwalner, Daniel Galvao, Ryan Cummings and Connor Ryan for their assistance with data collection.

REFERENCES

- [1] H. Kuehne, H. Jhuang, E. Garrote, T. Poggio, and T. Serre, "HMDB: A large video database for human motion recognition," in *2011 International Conference on Computer Vision*, 2011, pp. 2556–2563.
- [2] M. Amin, *Radar for Indoor Monitoring: Detection, Classification, and Assessment*. CRC Press, 2017.
- [3] S. Skaria, A. Al-Hourani, M. Lech, and R. J. Evans, "Hand-gesture recognition using two-antenna doppler radar with deep convolutional neural networks," *IEEE Sensors Journal*, vol. 19, no. 8, pp. 3041–3048, 2019.
- [4] P. Wang, W. Li, P. Ogunbona, J. Wan, and S. Escalera, "RGB-D-based human motion recognition with deep learning: A survey," *Computer Vision and Image Understanding*, vol. 171, pp. 118–139, 2018.
- [5] A. K. Seifert, M. G. Amin, and A. M. Zoubir, "Toward unobtrusive in-home gait analysis based on radar micro-doppler signatures," *IEEE Transactions on Biomedical Engineering*, vol. 66, no. 9, pp. 2629–2640, 2019.
- [6] J. Liu, C. Gu, Y. Zhang, and J. Mao, "Analysis on a 77 ghz mimo radar for touchless gesture sensing," *IEEE Sensors Letters*, vol. 4, no. 5, pp. 1–4, 2020.
- [7] M. G. Amin, Y. D. Zhang, F. Ahmad, and K. C. D. Ho, "Radar signal processing for elderly fall detection: The future for in-home monitoring," *IEEE Signal Processing Magazine*, vol. 33, no. 2, pp. 71–80, 2016.
- [8] G. Gennarelli, F. Soldovieri, and M. Amin, "Radar for indoor surveillance: state of art and perspectives," in *Multimodal Sensing: Technologies and Applications*, E. Stella, Ed., vol. 11059, International Society for Optics and Photonics. SPIE, 2019, pp. 1 – 10. [Online]. Available: <https://doi.org/10.1117/12.2527660>
- [9] S. A. Shah and F. Fioranelli, "RF sensing technologies for assisted daily living in healthcare: A comprehensive review," *IEEE Aerospace and Electronic Systems Magazine*, vol. 34, no. 11, pp. 26–44, 2019.
- [10] B. Jokanović and M. Amin, "Fall detection using deep learning in range-doppler radars," *IEEE Transactions on Aerospace and Electronic Systems*, vol. 54, no. 1, pp. 180–189, 2018.
- [11] S. Z. Gurbuz and M. G. Amin, "Radar-based human-motion recognition with deep learning: Promising applications for indoor monitoring," *IEEE Signal Processing Magazine*, vol. 36, no. 4, pp. 16–28, 2019.
- [12] Z. Chen, G. Li, F. Fioranelli, and H. Griffiths, "Dynamic hand gesture classification based on multi-static radar micro-doppler signatures using convolutional neural network," in *2019 IEEE Radar Conference (RadarConf)*, 2019, pp. 1–5.
- [13] F. Fioranelli, J. Patel, S. Z. Gürbüz, M. Ritchie, and H. Griffiths, "Multistatic human micro-doppler classification with degraded/jammed radar data," in *2019 IEEE Radar Conference (RadarConf)*, 2019, pp. 1–6.

- [14] S. Gurbuz, J. Soraghan, A. Balleri, and C. Clemente, "Micro-doppler based in-home aided and unaided walking recognition with multiple radar and sonar systems," *IET Radar, Sonar & Navigation*, vol. 11, 06 2016.
- [15] L. Cohen, "Time-frequency distributions-a review," *Proceedings of the IEEE*, vol. 77, no. 7, pp. 941–981, 1989.
- [16] P. Flandrin, *Time-Frequency/Time-Scale Analysis*. Academic Press, 1999.
- [17] V. Chen and H. Ling, *Time-Frequency Transforms for Radar Imaging and Signal Analysis*. Artech House, 2002.
- [18] P. Setlur, M. Amin, and F. Ahmad, "Analysis of micro-Doppler signals using linear FM basis decomposition," in *Radar Sensor Technology X*, R. N. Trebits and J. L. Kurtz, Eds., vol. 6210, International Society for Optics and Photonics. SPIE, 2006, pp. 201 – 211. [Online]. Available: <https://doi.org/10.1117/12.669003>
- [19] B. Erol and M. Amin, "Generalized PCA fusion for improved radar human motion recognition," in *2019 IEEE Radar Conference (RadarConf)*, 2019, pp. 1–5.
- [20] A. Malhi and R. X. Gao, "PCA-based feature selection scheme for machine defect classification," *IEEE Transactions on Instrumentation and Measurement*, vol. 53, no. 6, pp. 1517–1525, 2004.
- [21] M. G. Amin and R. G. Guendel, "Radar human motion recognition using motion states and two-way classifications," in *2020 IEEE International Radar Conference (RADAR)*, 2020, pp. 1046–1051.